ARCHIVES OF METALLURGY AND MATERIALS
Volume 51 2006 Issue 3

K. ONOPIAK*, J. BOTOR*

SOLID OXIDE INCLUSIONS REFINING FROM MOLTEN ALUMINIUM BY BARBOTAGE

RAFINACJA CIEKŁEGO ALUMINIUM OD STAŁYCH WTRĄCEŃ TLENKOWYCH METODĄ BARBOTAŻU

Mechanism of removing oxide inclusions using inert gas flotation method based on water mineral processing systems was described. A selection of physicochemical data for calculation has been made. In the mechanism description many factors in the field of solid particle and gas bubble interaction in the molten aluminium phase were discussed, namely: bubble velocities and diameters, hydrodynamic conditions of the flotation process and its time connected parameters, probabilities of inclusion collision and adhesion to the bubble surface. A simple mathematical model describing the process of removing alumina inclusions from molten aluminium by barbotage was developed. The solid oxide particle removal efficiency in time was described based on hydrodynamic conditions. Influence of the refining gas bubble diameter was also discussed.

Presented mathematical model of the solid inclusions flotation with experimental results acquired on an industrial plant was verified. The plant consists of: periodically working crucible furnace for aluminium melting, URO-200 rotary impeller, Prefil footprinter melted metal quality analyzer and scanning microscope. Oxygenated with air or oxygen by the use of URO rotary impeller liquid A0 aluminium was refined in specified time limits for flow rate of argon averaging 10, 15 and 20 $dm^3\ min^{-1}$. Metal refining was performed for metal weight in the furnace from 180 to 250 kg, in the temperature range of 993–1023 K. Solid oxide removal efficiency was given by equation which is in keeping with adopted model i.e.: $\eta = 100(1-\exp(-0.00096t))$ where t is refining time.

Keywords: aluminium refining; oxide inclusions; barbotage; rotor; argon; alumina oxide

W pracy scharakteryzowano mechanizm usuwania wtrąceń tlenkowych metodą flotacji w oparciu o zjawiska zachodzące w systemach wzbogacania i flotacji rud. Przeprowadzono selekcję danych fizykochemicznych oraz dobrano niezbędne dane do przeprowadzenia obliczeń. W opisie mechanizmu uwzględniono szereg czynników w zakresie oddziaływania stałego wtrącenia z gazowym pęcherzykiem w fazie ciekłej, m.in.: prędkości wznoszenia i średnice pęcherzyków gazu; warunki hydrodynamiczne procesu i jego parametry czasowe oraz prawdopodobieństwa zderzenia i adhezji wtrącenia na powierzchni pęcherzyka.

Przedstawiono prosty model matematyczny procesu usuwania wtrąceń tlenku glinu z ciekłego aluminium metodą barbotażu. W wyniku przeprowadzonych obliczeń symulacyjnych, w uzależnieniu od warunków hydrodynamicznych, określony został stopień eliminacji stałych wtrąceń tlenkowych w czasie, jak również optymalna średnica pęcherzyków gazu rafinującego.

Scharakteryzowany matematyczny model procesu flotacji stałych wtrąceń tlenkowych zweryfikowano z danymi doświadczalnymi uzyskanymi na stanowisku przemysłowym składającym się z: pracującego cyklicznie pieca tyglowego do topienia aluminium, rafinatora barbotażowego typu URO 200, aparatury PREFIL określającej jakość metalu oraz mikroskopu skaningowego. Utlenione powietrzem lub tlenem technicznym za pomocą rotora rafinatora URO ciekłe aluminium w gatunku A0, poddawane było rafinacji w określonych przedziałach czasu, dla natężeń przepływu gazu rafinującego – argonu, wynoszących 10, 15 oraz 20 $dm^3\ min^{-1}$. Rafinację metalu przeprowadzano dla wytopów aluminium o masie 180–250 kg, w zakresie temperatur 993–1023 K. Sprawność usunięcia stałych wtrąceń opisano równaniem w postaci zgodnej z przyjętym modelem $\eta = 100(1 - \exp(-\ 0{,}00096\ t))$, gdzie t jest czasem rafinacji.

1. Introduction

Metals refining has crucial meaning for making goods of the demanded quality. For obtaining correct mechanical and physical product properties, metal should undergo the process of minimizing number of impurities. It is especially important in aluminium, because of its very high affinity to oxygen and there is a big difference between hydrogen capacity in liquid and solid aluminium. Studies analyzing the hydrogen desorption process from molten aluminium [1–7] were made, but similar analyses of removing solid nonmetallic inclusions are lacking.

* INSTITUTE OF NONFERROUS, 44-100 GLIWICE, 5 SOWIŃSKIEGO STR., POLAND

Aluminium refining is carried on by introducing inert gases (e.g. argon) into the melt. It happens by means of porous plugs, nozzles, rotary impellers. The choice of the proper method is dictated by high cleanliness demands and the production scale. Among described methods especially gas dispersion by rotors ensures a big interfacial area and good stirring, which makes the process fast and effective.

Impurities, which get connected with the bubble surface, are absorbed inside the gas bubble (e.g. hydrogen) or are adsorbed on the bubble surface (e.g. alumina oxide inclusions). Formulation of a simple mathematical aluminium refining model from solid nonmetallic inclusions could improve the process control range and effectiveness, which should enhance a final product quality.

2. Mechanism of removing oxide inclusions by inert gas flotation

We can divide the process of oxide inclusions flotation into:

1. introduction of the bubble into liquid metal and its movement to the inclusion
2. formation of a thin liquid film between inclusion and gas bubble
3. oscillation and/or sliding of the solid particle on the bubble surface
4. drainage and rupture of the film with the formation of a dynamic three – phase contact (TPC)
5. stabilization of the bubble – inclusion aggregate
6. flotation of the bubble – inclusion aggregate to the metal surface.

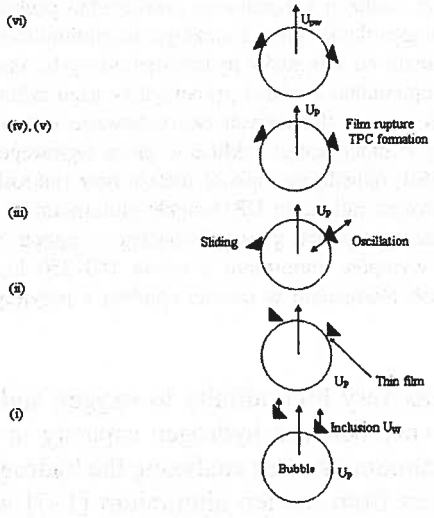

Fig. 1. Subprocesses of particle removal by bubble flotation in mineral processing

Figure 1 shows basic stages mentioned above, that is removing solid oxide inclusions in the bubble flotation process. We assume that inclusion – bubble interaction mechanism in high temperatures is similar to the one we meet in water based mineral processing systems. Injected into the liquid aluminium gas bubble is approaching the inclusion, where after the thinning and rupture of the intervening film, the inclusion adhesion on the bubble surface can follow. If inclusion doesn't slide away, the union bubble – inclusion must succeed. Simultaneously with the three – phase contact line formation, which is a bubble – inclusion contact area perimeter, the bubble – inclusion aggregate stabilization with respect to the external stresses comes after. Such aggregate is floated to the metal surface.

3. Model for solid oxide inclusion removal from molten aluminium by bubble flotation

3.1. Assumptions and equations selection

The process complexity influences description of available in literature models of aluminium refining from nonmetallic inclusions. Described models are simplified [8, 9, 10, 11]. To make a reasonable description of the process it was necessary to take under consideration only a few of the most influential factors. In this paper, a model of molten metal refining from oxide inclusions was based on the following assumptions:

1. the bubbles rise with fixed velocity and they are uniformly distributed in the liquid metal
2. bubbles diameters are of identical size and their quantity depends on gas flowrate and nozzle diameter
3. inclusions are evenly distributed in a molten metal volume and they do not have influence on bubbles movement
4. inclusions are removed only via flotation mechanism, excluding floating, collision and coagulation of solid particles
5. inclusion is considered to be removed from liquid aluminium when stable attachment occurs between gas bubble and solid inclusion
6. the system turbulence is disregarded
7. mechanism of the process is in accordance with a description in the chapter 2.

For characterizing metal refining process from inclusions, the equation describing solid oxides removal efficiency is needed. For that reason many physicochemical parameters and data were analyzed. On the basis of this analysis, selection of equations used farther in the paper was made:

a) equivalent refining gas bubble diameter used in the whole work was defined using [12] Davidson and Amick's (1) equation:

$$d_P = 0.54\left(Q_g\sqrt{d_d}\right)^{0.289}, \quad (1)$$

where: d_p – refining gas bubble diameter [m], Q_g – refining gas flowrate [$m^3\ s^{-1}$], d_d - rotary impeller nozzle diameter [m].

b) bubble velocity was described by [13] Davies and Taylor's (2) equation:

$$U_P = 1.02\left(\frac{gd_P}{2}\right)^{1/2}, \quad (2)$$

where: U_p – rising gas bubble velocity [$m\ s^{-1}$], g – gravitational acceleration [$m\ s^{-2}$]

c) for inclusion velocity equation (3) was used according to [14]:

$$U_W = \left(\frac{g(\rho_W - \rho)}{9\eta_C^{0,5}\rho^{0,5}}\right)^{2/3} d_W \quad \text{for} \quad Re_W < 1000, \quad (3)$$

where: U_w – inclusion velocity [$m\ s^{-1}$]; d_w – inclusion diameter [m]; η_C – liquid metal dynamic viscosity [Pa s]; ρ – densities of [$kg\ m^{-3}$]: ρ – liquid aluminium, ρ_w – alumina oxide inclusion; Re_w – inclusion Reynolds number.

d) total inclusion – bubble attachment probability [15, 16, 17] was described by (4):

$$P = \frac{2U_P D}{9(U_P + U_W)Y}\left(\frac{d_W}{d_P}\right)^2 \left(\left[(X+C)^2 + 3Y^2\right]^{1/2} + 2(X+C)\right)^2. \quad (4)$$

e) constant parameters in equation (4) were given by (5), according to [16]:

$$D = \left(\left[(X+C)^2 + 3Y^2\right]^{1/2} - (X+C)\right)/3Y, \quad (5)$$

where: $X = \frac{3}{2} + 9\mathrm{Re}_P/\left(32 + 9.888\mathrm{Re}_P^{0.694}\right)$

$Y = 3\mathrm{Re}_P/\left(8 + 1,736\mathrm{Re}_P^{0.518}\right)$

$C = (U_W/U_P)(d_P/d_W)^2$.

f) liquid aluminium density in temperature range from 933 to 1173 K was given by Gebhardt's equation [18]:

$$\rho = (2.368 - 2.63(T - T_t)10^{-4})1000. \quad (6)$$

Based on the above assumptions the following equations were characterized. The collision number of the bubble:

$$N_Z = V_P P n = \frac{\pi}{4} d_P^2 h_0 P n, \quad (7)$$

where: V_p – molten metal volume on the way of rising bubble [m^3], P – total bubble inclusion attachment probability, n – inclusion number in aluminium after refining time t, h_0 – melt bath height [m].

Number of the bubbles supplied to the liquid aluminium per unit time per unit volume of metal is:

$$N_P = \frac{6Q_g}{\pi d_P^3}\frac{1}{V}, \quad (8)$$

where: V – molten metal volume [m^3].

Total number of bubble – inclusion aggregates per time unit is described as:

$$N_C = N_Z N_P = \frac{3}{2}\frac{h_0}{V}\frac{P}{d_P}Q_g n = Zn, \quad (9)$$

where:

$$Z = \frac{3}{2}\frac{h_0}{V}\frac{P}{d_P}Q_g. \quad (10)$$

The rate of inclusion removal can be represented as:

$$-\frac{dn}{dt} = Zn. \quad (11)$$

Integrating between time limits $t = 0$ ($n = n_0$) and $t(n = n)$ gives:

$$n = n_0 \exp(-Zt). \quad (12)$$

The percentage removal efficiency of inclusion at time t is defined as:

$$\eta = 100\left(\frac{n_0 - n}{n_0}\right)$$

or

$$\eta = 100(1 - \exp(-Zt)). \quad (13)$$

3.2. Exemplary model calculation

The results of the model simulation are shown in Fig. 2, 3 and 4. For the calculation, fixed bubble diameter was assumed – Fig. 2 and 4. Calculation was made for the conditions: aluminium mass m = 200 kg, height of liquid metal h_0 = 0.455 m, aluminium viscosity in T = 1008 K was η_{Al} = 0.003 Pa s.

The rise in a removal efficiency of inclusions due to increased gas flowrate is shown in Fig. 2. Fig. 3 shows that small bubbles are the most effective for inclusion removal. The removal of inclusions under 20 μm diameter is especially difficult and could be done in more than 90% by bubbles smaller than 10 mm in diameter. Inclusions under 5 μm and smaller are successfully removed by bubbles of a diameter under 4 mm. Longer refining time increases inclusion removal efficiency – Fig. 4. Smaller solid particles refining lasts longer.

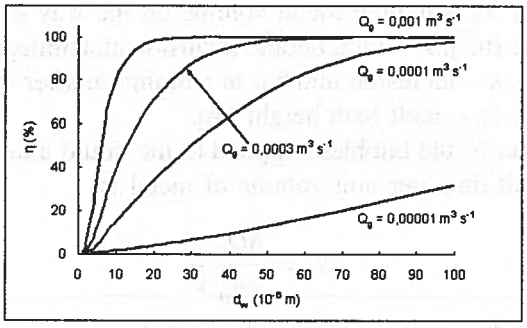

Fig. 2. The effect of refining gas flowrate on oxide inclusion removal efficiency from liquid aluminium depending on inclusion diameter d_W for equivalent bubble diameter d_P = 15 mm after refining time t = 1500 s.

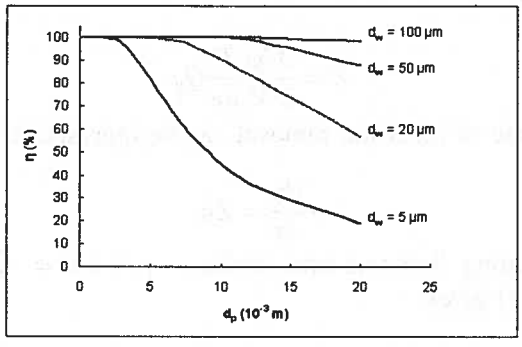

Fig. 3. The effect of refining gas bubbles diameters on inclusion removal efficiency for shown inclusion diameters d_W at gas flowrate Q_g = 0.0003 m^3 s^{-1} and after refining time t = 1500 s.

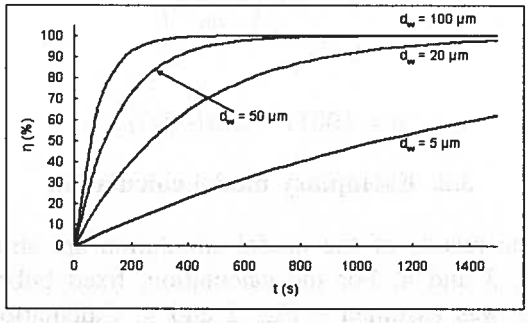

Fig. 4. The effect of refining time on inclusion removal efficiency for shown inclusion diameters d_W at gas flowrate Q_g = 0.0003 m^3 s^{-1} and after refining time t = 1500 s.

4. Experimental part

The results of a refining process research using periodically working rotary impeller URO-200 are discussed. The effectiveness of solid oxide inclusion removal from liquid aluminium applying Prefil Footprinter analyzer of melted metal quality, was estimated.

4.1. Instruments

A test was done on an industrial plant, which included:

- 300 kg capacity crucible furnace,
- periodically working URO-200 rotary impeller illustrated in Fig. 5
- Prefil footprinter liquid metal quality analyzer (Fig. 6)

A crucible furnace was equipped with a molten metal temperature regulation system making possible to maintain the needed temperature in range ±5 K.

Refining with rotary impeller shown in Fig. 5 is based on creating a flow of inert gas bubbles in molten aluminium. An impeller equipped with 8 nozzles of 0.002 m diameter each, is running at 400 rpm, breaking the bubbles into smaller ones and distributing them in the metal volume evenly. A bigger number of small bubbles result in a greater gas – metal interfacial contact area which brings on a higher ratio of inclusions adherence to the bubbles surface. Then the inclusions are floated to the metal surface. Inert gas is supplied to the nozzles by control system, which allows adjusting the gas flowrate for fluent in the range 0 to 25 dm^3 min^{-1}.

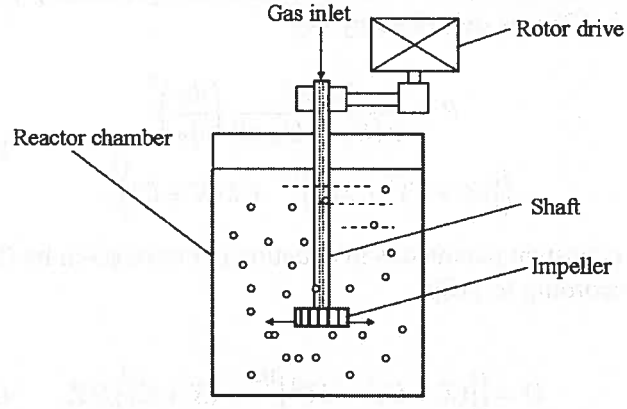

Fig. 5. 5 URO 200 plan

Performance of Prefil analyzer – Fig. 6 – is based on measurement of the mass of filtered liquid metal. Metal flow through a porous filter disc placed in the crucible bottom is forced by pressure. A load cell connected to a computer, records the filtered metal weight as a time function in periods of 3 s. The filtration curve is displayed on the computer's screen in the real time.

4.2. Materials parameters

In refining A0 quality aluminium, which contains at least 99.7% mass Al was used. According to analysis the impurities number was (mass %): Fe – 0.25%, Si –

0.2%, Cu, Mn, Mg and Ti maximally 0.03% each, Zn to 0.07%.

Oxidized metal was refined at Ar (99.999 mass %) flowrate amounting 10, 15 and 20 $dm^3\ min^{-1}$. Melt bath height h0 in furnace crucible accordingly to aluminium mass was 0.42-0.55 m. Aluminium refining and oxidizing was performed at an average temperature of 1008 ± 15 K. Liquid metal density was 2348 kg m^{-3} and its viscosity was of 0.003 Pa s.

4.3. Experiment

Molten aluminium was oxidized via rotary impeller for 10 minutes each time by air or oxygen at 10 $dm^3\ min^{-1}$ flowrate. Such oxidized metal was refined in research plant presented in point 4.1. Main parameters of 8 done tests: oxidizing – refining, are shown in Table 1. First column shows test marks in a succession from P1 – P8. Oxidized and refined metal mass at a presented gas flowrate Q_g during the given test is shown in column '2' and '3'. For each test there was a specified number of refining given in column '4'. After refining which lasts minimum 20 to maximum 1500 s and dross skimming, metal samples were taken for Prefil analyses, which marks are mentioned in the last column of Table 1. Samples were taken immediately after oxidizing and after 10 minutes of each refining period.

In Fig. 6 the molten metal analyzing method using Prefil – Footprinter device is shown. Firstly aluminium sample is poured into the warmed up crucible placed in the pressure chamber. Equipped with thermocouple pressure chamber lid is closed and than prescribed filtration temperature is reached. At the time the constant pressure forces metal to flow through ceramic filtration disc. Recorded aluminium mass rise is presented on line during filtration on computer's screen in the form of a filtration curve. Maximum filtration time is 150 s and then automatic chamber decompression makes possible to take the worn filtration disc out of the chamber and analyze it metallographically. For all samples filtration started at 983 K, under the fixed pressure of 83 kPa in the pressure chamber with the crucible inside. Filtration time and final metal mass in load cell depends on inclusions quantity contained in an aluminium sample. The more solid inclusions, the faster filtration disc blocking, and as a result, the smaller final mass of filtered metal. The graphical result of above is the bigger filtration curve slanting – liquid metal mass in dependence on filtration time. The better alloy cleanliness the shorter filtration time – less than 2 minutes – and metal mass in a load cell can reach nearly 1.5 kg.

TABLE 1

Main parameters of aluminium refining from nonmetallic inclusions

Test	m (kg)	Q_g ($dm^3\ min^{-1}$)	Number of refining during test	Operation markings
P1	180	10	5	K 11–17
P2	250	15	3	L 1, L 2, L 5–7
P3	220	15	3	L 8, L 10–13
P4	247	20	2	L 40, L 43–45
P5	220	20	3	L 46–50
P6	190	20	3	L 50, L 61–64
P7	202	10	1	L 70–74
P8	180	15	2	L 82, L 90–92

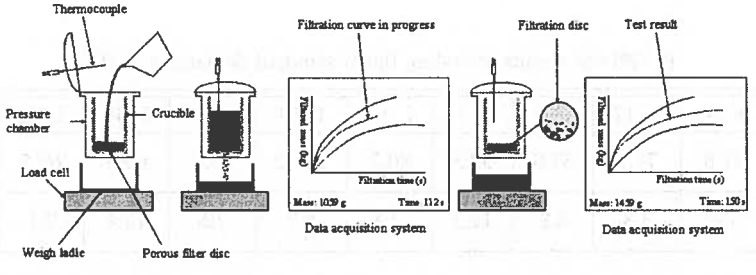

Fig. 6. Prefil Footprinter – ABB Bomem Inc. [19] – operation steps

Exemplary acquired filtered aluminium results in dependency on filtration time are presented in Fig. 7. During first test – P1 – Fig. 7, where consecutive samples analyzed on filtration apparatus Prefil were marked as K 11 to K 17, five refining operations were done. After pure aluminium sample taking (sample K 11), metal was oxidized (K 12) and than refined for: 20 s (K 13), next 20 s (K 14), in 2 minutes (K 15), finally finishing that test with two 10 minute refining cycles (K 16 and K 17).

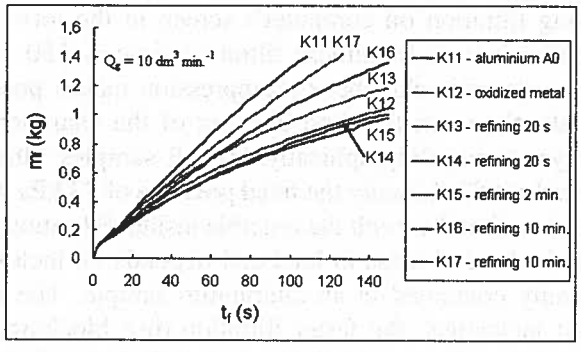

Fig. 7. Aluminium masses filtered through Prefil apparatus filter in time, after refining test P1 (samples K 11 – K 17)

5. Comparison of experimental results with mathematical model

The calculation results done on the basis of data acquired from Prefil device describing inclusion removal from molten aluminium efficiency in a refining time dependence is shown in Fig. 8. Values representing solid oxide removal efficiency with their standard deviation in accordance with samples marks are given in Table 2. Calculation was done by converting proportionally the filtered metal mass and taking its increasing or decreasing as proportional increase or decrease in inclusion removal efficiency after refining. In the other words bigger aluminium mass filtered through Prefil's filter, means higher solid inclusions removal efficiency and lower impurities level remaining in liquid metal volume. The most inclined curves on Prefil diagrams were treated as this showing aluminium condition after oxidizing. Therefore in Fig. 7 state of oxidized metal is represented by K 15 curve.

Results acquired from curves: K 16 and 17 (test P 1), L 6 and 7 (test P 2), L 12 and 13 (test P 3) and others were placed on the time scale, taking under consideration the total time of realized refining operations. It means that e.g. result for sample L 6 was localized in Fig. 8 for refining time amounts 840 s, covering L 5 result made before. Curves following results for sample L 5, i.e. L 6 and L 7 make possible charting aluminium refining coarse in test P 3.

For tests P 1 and P 2 inclusion removal efficiency at refining gas flowrate Q_g accordingly 10 and 15 dm^3 min^{-1}, after several minutes of refining was about 40%. Therefore acquired nearly 70% solid oxide inclusion removal efficiency for samples L 48 and L 62 just after 5 minutes are result of applied higher gas flowrate amounting 20 dm^3 min^{-1}. For this reason from tests P4 – P8 only results for samples L 44, 72 and 91 were placed in Fig. 8.

Approximating curve describing inclusion removal efficiency shown in Fig. 8 is given as:

$$\eta = 100(1 - \exp(-0.00096t)). \quad (14)$$

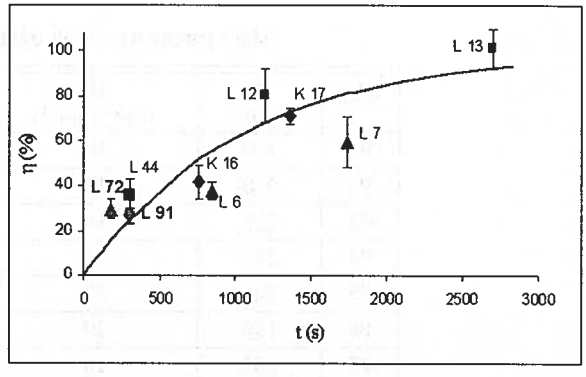

Fig. 8. Inclusions removal efficiency from molten aluminium in dependency on refining time with its standard deviations for tests P 1–8

TABLE 2

P1–P8 test results including theirs standard deviations in (%)

Sample	K 16	K 17	L 6	L 7	L 12	L 13	L 44	L 48	L 62	L 72	L 91
η (%)	41.8	71.1	37.9	59.3	80.2	101.2	35.7	69.5	69.5	29.7	26.6
s(η) (%)	7.6	3.8	4.2	11.3	11.8	8.7	7.5	12.4	7.1	4.5	3.3

The above curve is in keeping with model adopted in chapter 3. Data acquired from the mentioned curve are given in Table 3. The data result in that along with extending refining time it is harder to achieve higher level of inclusion removal efficiency from liquid aluminium.

TABLE 3

Selected results of inclusions removal efficiency η after refining time t from approximating curve places in Fig. 8

t (s)	600	900	1500	2100	2400	2700
η (%)	43.8	57.9	76.3	86.7	90.0	92.5

For the acquired low level solid fine impurities average inclusion removal efficiency after 5 minutes refining transcends 25%. After the following 25 minutes of refining above 76% of solid oxides is removed, but for removing next several % of inclusions additional 20 minutes barbotage refining is needed. Nearly a half of solid inclusions is removed during the first 10 minutes of refining. Standard deviation of approximation curve calculated on the basis of a difference between experimental values and the curve course amounts to 12.5%.

Model curves calculated for: aluminium mass m = 220 kg, at its density ρ = 2348 kg m^3, at the temperature T = 1008 K, at metal bath height h_0 = 0.49 m and its viscosity η_{Al} = 3.0 cP, for inclusion diameters varied from 5 μm to 100 μm, which are juxtaposed with described above experimental curve is shown in Fig. 9. The seen values are similar to average experimental results.

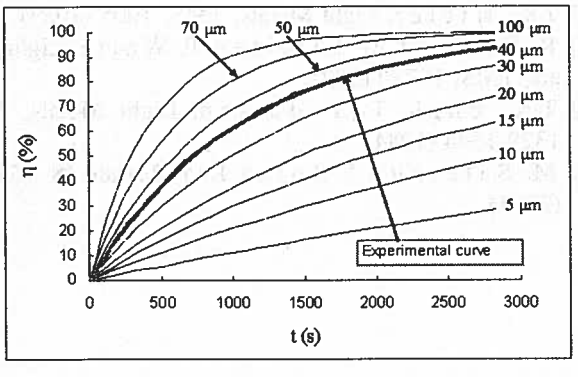

Fig. 9. Juxtaposition of curves acquired from model calculation for shown inclusion diameters in [μm] at gas flowrate Q_g = 15 dm^3 min^{-1} and bubble diameter d_P = 0.0200 m with experimental curve for tests P 11–8

The experimental curve course indicates probable removed inclusions diameter range varied from 30 μm to 50 μm. Tests curve slant is similar to model curves course.

6. Discussion and conclusions

In this paper liquid aluminium refining from solid oxide inclusions was discussed.

Calculation results confirm that acquired inclusion removal efficiency level is similar to experimental data obtained in industrial conditions. Tests curve η = f(t) shape and slant is similar to model curves. Comparison done between them for different inclusion diameters localized tests equation in range 30 to 50 μm. Such inclusion diameter d_W is possible. The above proves that accepted model is similar to real conditions. But we must remember that:

1. The model was developed using equations valid in water based flotation systems
2. Simplifying assumptions were taken
3. Assessment of inclusion number change was made upon half-number. Acquired results could be treated as half-number.

Used barbotage method by rotary impeller gave in about 15 minutes approximately 60% of removed inclusions. Such result is sufficient for most technological applications. In case of making very high quality products e.g. aluminium foils, additional filtration operation is needed. Tests results support acquiring a good level of oxide inclusion removal. It means that achieved cleanliness level is in accord with such applied in the world devices like (inclusion removal efficiency [%]): ASV (40-90%) [20, 21], Alpur (60-95%) [22, 23, 24], AFD (do 90%) [25]. Simultaneously there can be observed a correspondence in the course of aluminium refining curves from inclusions and hydrogen, where in both cases about 50% of solid and gaseous impurities is removed during the first 10 minutes of the process [26, 27].

A difficult removal of small inclusions, which arose after oxidizing the melt in a high turbulence condition, is contributing to prolonging liquid metal refining time. Therefore 45 minutes long refining time needed for achieving almost 93% aluminium purity from inclusions level shown in Fig. 8 is a result of presence of a high number, hardly removing small solid inclusions of very high dispersion in a melt. Such deep liquid metal clearance is not applied in industrial practice. Practically applied aluminium refining times from hydrogen and accompanied to it inclusions reach 10–15 minutes. Such time period allows on effectively realized metal refining from most inclusions, especially that of a diameter higher than 20 μm. Experimental curve equation describing inclusion removal efficiency from liquid aluminium for test P 1 – P 8 at standard deviation amounting 12.5% given as (14):

$$\eta = 100(1 - \exp(-0,00096t))$$

can be applied for metal refining from large number of small solid inclusions arisen in conditions similar to described. Equation was set for gas flowrate Q_g = (15 ± 5) $dm^3\ min^{-1}$. This equation has a similar character to the described in the paper refining model that covered mainly a flotation aspect of the process.

Mechanism of liquid aluminium refining from solid inclusions is complex but it can be ascertained that flotation has decisive influence on its course. The discussed mechanism describing phenomena in water based systems of mineral processing must not be confirmed in liquid metallic phase. The reason of that are elementary differences between features of mentioned systems, namely: temperatures, viscosities, densities, surface and interfacial tensions.

An advantage of applied metal quality evaluation method is a possibility of analyzing online a big, mildly symptomatic sample in the liquid phase. Prefil test excludes atmosphere influence, too. Difficulties in real change assessment of inclusion number develop from lack of Al_2O_3 inclusions quantity analyzing method. It comes from inaccessibility of chemical method and irregular solid inclusion dispersion in liquid metal. Method disadvantage is results dependence on inclusion size, too.

Acknowledgements

The research was partially supported by the Polish Department for Education and Science. Grant No. 4 T08B 018 24.

REFERENCES

[1] J. Botor, Prace IMN Dodatek, **7** (1), 3 (1978)
[2] G.K. Sigworth, T.A. Engh, Metall. Trans. B, **13B**, 447 (1982)
[3] W. Geller, Z. Metallkd. **35**, 213 (1943)
[4] R.D. Pelhke, A.I. Bement: Trans. AIME **224**, 1237 (1962)
[5] J. Botor, Metal. Odlewn. **6**, 21 (1980)
[6] J. Botor, Aluminium **56**, 519 (1980)
[7] J.A. Dantzig, J.A. Clumpner, D.E. Tyler, Metall. Trans. B **11B**, 433 (1980)
[8] V.G. Levich, Physicochemical hydrodynamics, Prentice-Hall, Englewood Cliffs, (1962)
[9] A.G. Szekely, Met. Trans. B **7B**, 259-270 (1976)
[10] S.T. Johansen, A. Fredriksen, B. Rasch, Light Metals, 1203-1206 (1995)
[11] T.A. Engh, Principles of Metals Refining, Oxford University Press, Oxford (1992)
[12] L. Davidson, E.H. Amick Jr., AIChE Journal **2**, 337 (1956)
[13] R.M. Davies, G.I. Taylor, Proc. Roy. Soc. A 200, 375 (1950)
[14] F. Oeters, Metallurgy of steelmaking, Berlin, VSHD (1994)
[15] A.V. Nguyen, H.J. Schulze, J. Ralston, Int. J. Miner. Process. **53**, 225 ÷ 249 (1998)
[16] A.V. Nguyen, S. Kmet, Int. J. Miner. Process. **40**, 155 ÷ 169 (1994)
[17] A.V. Nguyen, S. Kmet, Int. J. Miner. Process. **35**, 205-223 (1992)
[18] E. Gebhardt, M. Becker, S. Dorner, Aluminium, **31**, 315 (1955)
[19] Prospekt informacyjny firmy ABB Bomem Inc. — urządzenie Prefil — tester czystości ciekłego metalu
[20] M. Nilmani, P.K. Thay, C.J. Simensen, Light Metals, TMS 939 (1992)
[21] E. Myrbostad i in., Light Metals, TMS, 861 (1986)
[22] J. Bildstein, I. Ventre, Light Metals, TMS 755-763, (1990)
[23] J. Bildstein, J.M. Hicter, Light Metals, TMS, 1209 (1985)
[24] J.M. Hicter, Light Metals, TMS, 1005 (1983)
[25] R. Dumont, M. Litalien, P. Waite, Light Metals, TMS, 1077 (1992)
[26] T.A. Engh, T. Pedersen, Light Metals, TMS, 1329-1344 (1984)
[27] M. Saternus, J. Botor, Rudy Metale **48**, 154-160 (2003)

Received: 10 February 2006.